communications biology

A Nature Portfolio journal

Article

https://doi.org/10.1038/s42003-025-08946-4

Engineering a heparin-mimetic biomaterial to promote tissue vascularization

Linqing Li[1,2,3,10] ✉, Jinling Yang[1,2,10], Luba Perry[2], Jennifer L. Bays[1,2], Sangeeta N. Bhatia[2,4,5,6,7,8,9], Jeroen Eyckmans[1,2] & Christopher S. Chen[1,2] ✉

A major challenge in tissue engineering involves the development of synthetic biomaterials that effectively induce and maintain functional vascularization of engineered tissue constructs post implantation. While conjugating heparin to a dextran hydrogel developed a pro-angiogenic scaffold that led to substantial endothelial multicellular assembly in vitro and enhanced host vessel invasion in vivo, the inherent anti-coagulant bioactivities of native heparin elicited substantial local bleeding upon implantation. To decouple the pro-angiogenic effects from the anti-coagulant activity, we developed a synthetic, heparin-mimetic material by introducing sulfate adducts to the dextran backbone. These heparin-mimetic hydrogels bound and immobilized growth factors, enhanced angiogenic signaling, and promoted both in vitro vascular network formation in 3D and in vivo tissue microvascularization to a similar extent as heparin conjugated hydrogels, but without inducing local bleeding at implantation sites. This development of a fully synthetic, highly tunable angiogenic biomaterial provides a new material system to engineer functional vascularized tissues.

Establishing a functional vasculature that supplies sufficient oxygen and nutrient exchange is essential for maintaining tissue function and ensuring engraftment of engineered constructs after implantation, which remains one of the greatest challenges in regenerative medicine[1–3]. Numerous biomaterials, both natural and synthetic, such as fibrin[4], collagen[5], hyaluronic acid[6], polyethylene glycol[7], alginate, and chitosan[8] have been widely employed to support angiogenesis in tissue engineering[3,9,10]. These materials often provide a permissive environment for endothelial cell adhesion, migration, and initial sprouting. However, in most cases, these biomaterials alone, without incorporation of biochemical cues or cells, are insufficient to support robust, stable, and mature vascular network formation[11]. While exogenous delivery of angiogenic growth factors can enhance vascularization[12], the effect is often transient due to the rapid clearance of these diffusible factors from the biomaterial, resulting in short-lived angiogenic responses[9,13]. Strategies involving covalent conjugation[14] or affinity-based tethering[15] of growth factors to biomaterials have substantially improved angiogenic outcomes[16–20]. However, these approaches require careful optimization of the immobilization chemistry and biomaterial system to preserve bioactivity and ensure sustained efficacy.

Given the intrinsic properties of native extracellular matrix (ECM) in angiogenesis[13,21,22], an alternative strategy has been to incorporate pro-angiogenic macromolecules, such as heparin, in biomaterials[23–25]. Heparin is a highly sulfated glycosaminoglycan (GAG) known to bind to a wide range of growth factors, chemokines, and ECM proteins[26–28]. It has been used in biomaterials for controlled protein release, anti-coagulation, immune modulation, and the promotion of angiogenesis[23,26,28–31]. Despite its encouraging results, native heparin, which is isolated from animal tissues, exhibits considerable batch-to-batch variations in disaccharide sequence, molecular weight, chemical structure, sulfation degree, and purity, making it difficult to develop as a reliable source for clinical applications[32,33]. Furthermore, while heparin is widely used as an anti-coagulant in clinical settings[34], its role in biomaterials is complex and can vary depending on

[1]Department of Biomedical Engineering and the Biological Design Center, Boston University, Boston, MA, USA. [2]Wyss Institute for Biologically Inspired Engineering, Harvard University, Boston, MA, USA. [3]Department of Chemical Engineering and Bioengineering, University of New Hampshire, Durham, NH, USA. [4]Harvard-MIT Division of Health Sciences and Technology Program, Institute for Medical Engineering and Science, Massachusetts Institute of Technology, Cambridge, MA, USA. [5]David H. Koch Institute for Integrative Cancer Research, Massachusetts Institute of Technology, Cambridge, MA, USA. [6]Department of Electrical Engineering and Computer Science, Massachusetts Institute of Technology, Cambridge, MA, USA. [7]Department of Medicine, Brigham and Women's Hospital and Harvard Medical School, Boston, MA, USA. [8]Broad Institute of Massachusetts Institute of Technology and Harvard University, Cambridge, MA, USA. [9]Howard Hughes Medical Institute, Chevy Chase, MD, USA. [10]These authors contributed equally: Linqing Li, Jinling Yang. ✉e-mail: Linqing.Li@unh.edu; chencs@bu.edu

factors such as material design and growth factor delivery strategy[35]. Its pro-angiogenic effects are largely attributed to its ability to bind and present growth factors; however, even when immobilized within a biomaterial, heparin still harbors localized anticoagulant activity. This residual activity, likely due to enzymatic exposure of bioactive domains at the implant-host interface, may transiently disrupt hemostasis, potentially interfering with wound sealing and early tissue integration. These context-dependent effects raise important considerations for its use in surgical applications and warrant further evaluation.

To overcome these limitations, we developed a dextran-based hydrogel platform with tunable biophysical and biochemical properties. We showed that while heparin conjugation enhanced vascular network formation and host vessel invasion, its anticoagulant activity induced local bleeding upon implantation. To eliminate this side effect, we engineered synthetic heparin-mimetic hydrogels by sulfating the dextran backbone. These hydrogels retained the ability to sequester growth factors, promote angiogenic signaling, and drive both in vitro and in vivo vascularization without bleeding complications, providing a fully synthetic system to engineer functional vascularized tissues.

Results and discussion

To develop a tunable biomaterial system that mimics heparin's pro-angiogenic activity while eliminating its drawbacks, we chose dextran, a homopolysaccharide commonly used in clinical settings, as a base material. Dextran is intrinsically biocompatible and bio-inert with no known cell surface receptor binding activity, and has structural features similar to the glycosylated layer of native extracellular matrices[36–38]. We created cell-interactive, biomimetic hydrogels by reacting methacrylate functionalized dextran macromers (Dex-MA) with di-thiolated metalloproteinase (MMP)-cleavable crosslinkers, and thiol-terminated RGD peptides *via* a Michael-type addition reaction (Fig. 1a)[39]. This synthetic system allows for the independent modulation of multiple material properties, including tunable hydrogel stiffness (ranging from ~200 to 4055 Pa by adjusting bulk material solution concentrations (from 2 to 4 wt%) or crosslinking density; Fig. 1b and Supplementary Fig. 1a, b), cell adhesiveness (through coupling varying concentrations of cell-adhesive RGD peptide; Supplementary Fig. 1c), and matrix degradation (by tuning MMP-labile crosslinker sequences; Supplementary Fig. 1c, d). To enhance angiogenesis, we chemically conjugated heparin to the dextran gels or physically mixed a soluble, non-modified heparin during hydrogel crosslinking as a control. The incorporation of either conjugated or soluble heparin into the dextran hydrogel did not affect the hydrogel crosslinking time, equilibrium modulus, or our ability to control materials properties (Fig. 1c, d).

Having established a tunable material platform, we next examined the effect of hydrogel composition and heparin incorporation on vascular network formation in vitro. To assess vasculogenesis, human umbilical vein endothelial cells (HUVECs) and human dermal fibroblasts (HDFs) were encapsulated in 3D and co-cultured within various dextran-based hydrogels. After 14 days, endothelial cells formed robust multicellular networks (Fig. 1e and Supplementary Fig. 2a), featuring higher densities of longer vessels with numerous branch points and defined lumen structures only in dextran gels conjugated with heparin and impregnated with vascular endothelial growth factor (VEGF) and basic fibroblast growth factor (bFGF) (cHep-MA+GFs). In contrast, hydrogels lacking heparin (Dex-MA+GFs), containing soluble heparin (sHep+GFs), or conjugated heparin without growth factors (cHep-MA) all failed to form interconnected vascular structures with a lower vessel density, vessel length, and reduced number of branch points (Fig. 1e, f and Supplementary Fig. 2b–d). To explore the impact of mechanical properties on vascular network formation, we repeated the co-culture experiments using hydrogels with a varying stiffness range (~ 405 to 4055 Pa, selected to represent a physiologically relevant stiffness range employed in prior hydrogel-based angiogenesis studies[16,40,41]), while maintaining the concentration of conjugated heparin and the supplemented GFs constant in dextran gels. We observed a stiffness-dependent vascular assembly: soft gels (~ 405 Pa) supported early multicellular connections, whereas stiff gels (~ 4055 Pa) resulted in minimal vascular formation. Interestingly, in the soft matrix, pre-formed vasculature eventually regressed, likely due to decreased mechanical integrity from rapid matrix degradation. Among tested conditions, intermediate stiffness (~ 2084 Pa) supported the most robust and stable vascularization (Supplementary Fig. 3), characterized by well-organized, interconnected vascular networks with long-term stability. These findings were further supported by an angiogenic sprouting assay, wherein encapsulated HUVEC spheroids exhibited varying degrees of sprouting and endothelial cell invasion depending on hydrogel compositions; cHep-MA+GFs hydrogel composition significantly enhanced more multicellular sprouts compared to all other gel formulations (Supplementary Fig. 4).

To evaluate whether these findings would translate in vivo, we implanted these materials subcutaneously in mice and assessed vascularization after 14 days. Compared to hydrogels without heparin (Dex-MA +GFs), those with soluble heparin (sHep+GFs), or those lacking growth factors (cHep-MA), the heparin-conjugated dextran with growth factors (cHep-MA+GFs) hydrogels induced significant invasion of host vasculature (Fig. 1g) and demonstrated the highest degree of vascularization as measured by the presence of CD31+ host endothelial cells (Fig. 1h). Moreover, these invading vessels featured hierarchical branching networks and established connectivity to the systemic circulation as demonstrated by the perfusion of 70 kDa FITC-dextran that was injected intravenously prior to tissue harvesting (Fig. 1i, j). While these initial studies confirmed that heparin conjugation in biomaterials is an effective strategy to enhance in vivo vascularization, we also observed that animals receiving heparin-containing hydrogels experienced persistent local bleeding during implantation and post-operatively at day 1 (Fig. 1k). Heparin-conjugated dextran gels induced significant bruising with an area approximately 162 mm^2 around the implantation sites, compared to the minimal bruising area (~ 11 mm^2) observed in dextran only gels (Fig. 1l), which in 30–50% of the cases resulted in impaired mobility and morbidity due to prolonged bleeding from the wounds. While this is an indirect measurement of local bleeding and is difficult to distinguish from the permeability of newly invading vessels, there is minimal to no host vessel invasion at this early time point (day 1). Therefore, the major contribution to the observed local bleeding is likely due to the leakage from surrounding host vessels caused by the presence of heparin. These early local bleeding at implantation sites resolved upon tissue harvesting at day 14 post implantation. The increased FITC-dextran signal (Fig. 1i, j) at day 14 suggests functional perfusion through intact host vasculature, rather than local bleeding. The proportionally decreased signal in Fig. 1i, j compared to Fig. 1g, h suggest that mCD31-positive but FITC-dextran-negative vessels likely represent immature or non-perfused structures, lacking lumen development or connectivity to the circulatory system, and are not necessarily indicative of leakage or increased permeability. Nevertheless, these observations highlight safety concerns of the risks of incorporating heparin for translational applications and prompted us to investigate the development of a synthetic heparin mimetic could recapitulate the observed pro-angiogenic benefits without the anticoagulant drawbacks of native heparin.

Heparin's ability to sequester growth factors and its pro-angiogenic properties are mediated by electrostatic interactions between the high charge density of its negatively charged sulfate groups[26–28,42]. However, its anticoagulant bioactivity is specifically controlled by the pentasaccharide sequence with eight sulfate residues that bind to antithrombin, inhibiting thrombin and co-factor Xa to reduce clot formation[27,28,43]. To decouple the anticoagulant activity from the pro-angiogenic properties, we hypothesized that introducing randomly distributed charged adducts along the dextran backbone via sulfation could achieve this (Fig. 2a). To test this, we employed a sulfur trioxide/DMF complex to sulfate the dextran[44]. The degree of sulfation could be tuned to yield highly sulfated dextran (HS-Dex-MA) with a sulfation level comparable to that of native heparin, as confirmed by the appearance of a purple color in the dimethylmethylene blue (DMMB) colorimetric assay (Fig. 2b) and by changes in zeta potential relative to soluble sHep and Hep-MA (Fig. 2c, HS-Dex-MA: -19.2 ± 2.6; soluble

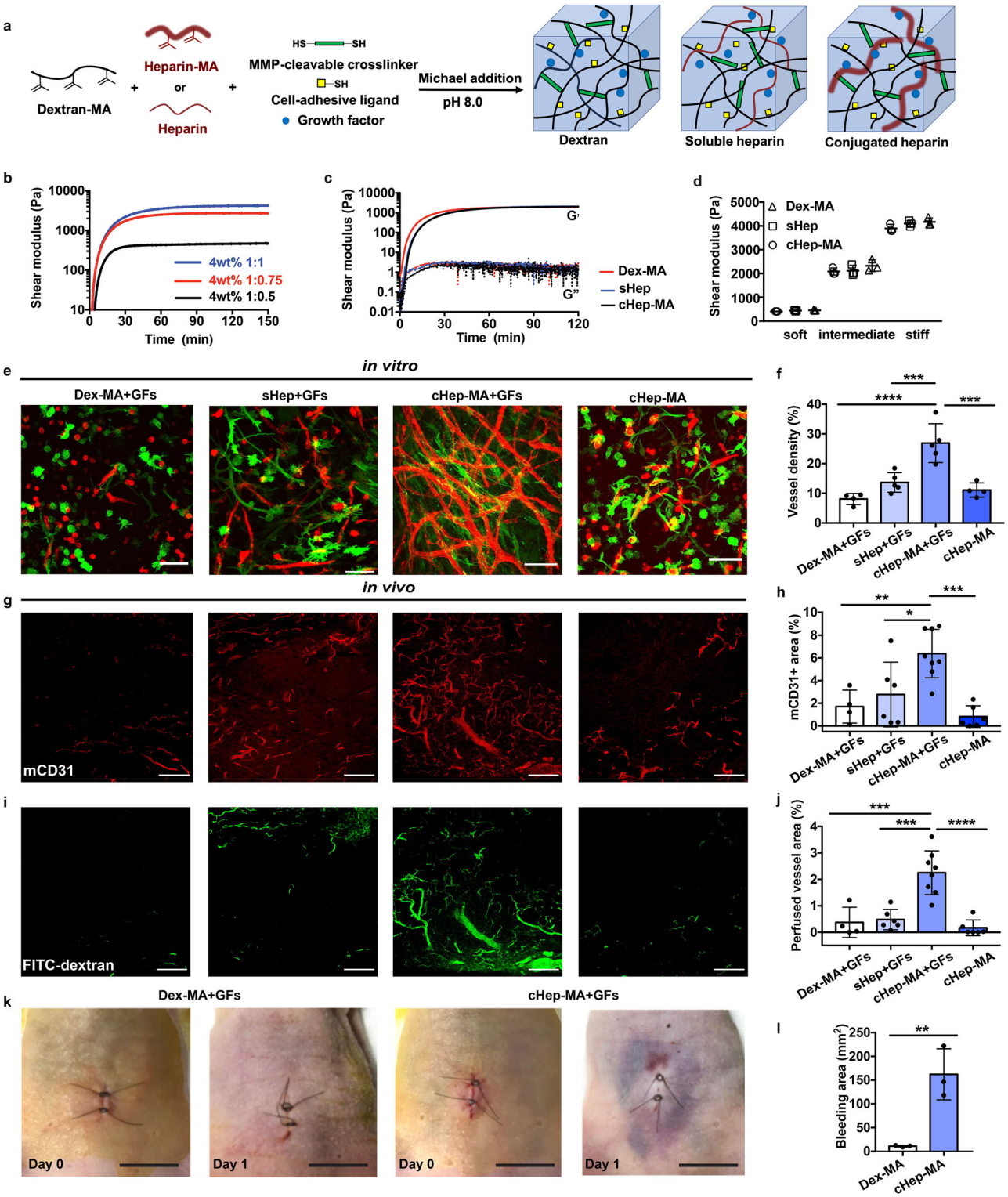

heparin: -20.5 ± 3.4; and Hep-MA: -31 ± 6.7). We also generated a lower sulfation dextran (LS-Dex-MA) with a significantly reduced zeta potential (-9.3 ± 2.6) to serve as a control in subsequent studies. Importantly, these chemical modifications did not affect the mechanical properties of hydrogels generated from sulfated dextrans, as demonstrated by oscillatory shear rheology exhibiting comparable storage moduli approximately 2000 Pa across all hydrogel compositions (Fig. 2e, f). Together, these data suggest that the extent of scaffold sulfation can be tuned independently of matrix stiffness.

To assess the effects of this new material on coagulation, we performed a mouse tail bleeding assay following systematic infusion through subcutaneously implanted osmotic mini-pumps. As expected, heparin significantly impaired blood coagulation and elicited a much longer clotting time (~ 8 mins) compared to saline (~ 2.2 mins) and unmodified dextran (~ 2.5 mins) conditions (Fig. 2d). In contrast, our synthetic heparin mimetic (sulfated dextran) did not alter clotting time (~ 2.5 mins). The key bioactivity of interest in heparin is its ability to enhance growth factor signaling[26,28,42,45]. To determine whether sulfated

Fig. 1 | Heparin conjugation in biomaterial enhances tissue vascularization but induces local bleeding in vivo. a Schematic representation of formulating synthetic and pro-angiogenic hydrogels containing Dex-MA co-crosslinked with either chemically conjugated heparin or soluble heparin, in the presence of thiolated cell-adhesive peptides and di-thiol terminated MMP-cleavage peptide crosslinkers *via* Michael-type addition reaction. **b** Oscillatory shear rheology time sweep of 4 wt% dextran hydrogel formulated with different crosslinking densities, yielding hydrogels with shear moduli from 454 Pa (soft, 1:0.5), 2326 Pa (intermediate, 1:0.75), to 4167 Pa (stiff, 1:1), conducted at 37 °C with frequency at 6.28 rad/s and 1% strain, $n = 3$. **c** Oscillatory shear rheology time sweep for in situ crosslinking dextran-based hydrogels with constant crosslinking density (intermediate, 1:0.75) but 10% (w/w) soluble and conjugated heparin in dextran gels; yielding comparable shear moduli between sHep ~2114 Pa and cHep ~2084 Pa groups, $n = 3$. Time sweep was conducted at 37 °C with frequency at 6.28 rad/s and 1% strain over 2 h. The viscoelastic properties of dextran-based hydrogels are represented by the storage modulus G' (solid phase, solid lines) and the loss modulus G" (liquid phase, dotted lines). **d** Mechanical properties of hydrogels formulated with varying material compositions and crosslinking densities to achieve tunable hydrogel stiffness, which was dependent on the crosslinking ratio rather than the material composition, $n = 3$. **e** Representative confocal fluorescent images showing 3D in vitro vascular network formation by co-culturing of Ruby-LifeAct-HUVECs and GFP-HDFs in dextran-based biomimetic hydrogels with different material compositions at day 14; dextran gels without heparin (Dex-MA+GFs, $n = 4$), dextran gels with soluble non-reactive heparin (sHep+GFs, $n = 5$), dextran gels with conjugated heparin (cHep-MA+GFs, n = 6) and dextran gels with conjugated heparin but without growth factors (cHep-MA, $n = 4$); scale bar, 100 μm. **f** Quantification of vessel density, defined by percentage of total endothelial cell area per image frame, $n \geq 4$. **g** Representative images of mouse CD31 staining from in vivo tissue samples with various material compositions harvested at day 14, scale bar, 200 μm. **h** Quantitative analysis of host blood vessels invading into dextran gels measured by the percentage of mCD31 positive area, $n \geq 4$. **i** Representative images of FITC-dextran signals of in vivo tissue samples with FITC-dextran (70 kDa) intravenously injected prior to harvesting hydrogels at day 14, scale bar, 200 μm. **j** Percentage of perfused host vessels quantified by FITC-dextran (70 kDa) positive area, $n \geq 4$. **k**) Representative images showing heparin-containing dextran gels induce local bleeding side effects post implantation at day 1, $n = 3$, scale bar, 1 cm. **l** Quantification of skin area showing local bleeding side effects induced by implantation of heparin-containing gels, $n = 3$. $^{*}P \leq 0.05$, $^{**}P \leq 0.01$, $^{***}P \leq 0.001$ and $^{****}P \leq 0.0001$. Scatter dot plots with error bars represent means with standard deviations.

dextrans when incorporated into hydrogels can enhance growth factor signaling, we cultured endothelial cells on various growth factor-laden hydrogels and examined the activation of VEGFR2, Akt and ERK1/2 – two key signaling pathways downstream of VEGF receptor signaling. Indeed, endothelial cells cultured on dextran gels with conjugated heparin or highly sulfated dextran (HS-Dex-MA) exhibited elevated and comparable levels of VEGFR2, Akt and Erk1/2 phosphorylation (Fig. 2g-j), as compared to all other hydrogel compositions, suggesting that our engineered sulfated dextran material retains the growth factor-enhancing activity of native heparin, but without the anticoagulant effects.

Having determined that sulfated dextran can serve as a potential heparin analogue that preserves growth factor signaling effects without anticoagulant bioactivity, we next tested whether sulfated dextran hydrogels support vascularization. We first assessed this possibility using the established sprouting and vasculogenesis assays. Hydrogel containing HS-Dex-MA induced the formation of extensive vascular networks and substantial angiogenic sprouting (Fig. 3a–d), characterized with a vessel density of 31.0 ± 6.7%, an average vessel length of 258.9 ± 72.4 μm, number of branch points at 32 ± 7, and a higher number of sprouts (Fig. 3e–h). These values of key angiogenic parameters were comparable to those observed in the heparin-conjugated hydrogels (Fig. 1e, f, and Supplementary Fig. 2b–d) and significantly higher than all other control conditions. LS-Dex-MA hydrogels exhibited markedly reduced metrics, including vessel density (13.2 ± 4.0%), average vessel length (106.3 ± 21.2 μm), and number of branch points (6 ± 2). Interconnected lumens were observed in the self-assembled microvasculature (Fig. 3i) and these structures persisted and maintained vascular integrity in sulfated dextran hydrogels for over a month in culture (Fig. 3j).

Lastly, we investigated whether the sulfated dextran-based material could support angiogenesis without inducing local bleeding in vivo. Using the same mouse subcutaneous model, we observed that both low and highly sulfated dextran gels did not cause bleeding post-implantation at day 1 (Fig. 4a, b). However, highly sulfated dextran gels enhanced significant angiogenesis, as demonstrated by substantial host endothelial network invasion in tissue sections (Fig. 4c, d) and perfusion visible by intravenously injected FITC-dextran (Fig. 4e, f and Supplementary Fig. 5). In contrast, gels with low sulfation compositions did not elicit similar effects. Importantly, we did not observe any evidence of microvascular bleeding, bruising, or impaired mobility in animals exposed to the sulfated dextran hydrogels upon implantation. Collectively, these data suggest that we have successfully developed a synthetic heparin mimetic that lacks anticoagulation activity without compromising the activity to promote tissue vascularization.

Extracellular matrices are rich in proteoglycans and GAGs, which are charged molecules known for binding to a variety of GFs, cytokines and morphogens critical for regulating cell behavior and function[46–48]. Among GAGs, native heparin is the most negatively charged and sulfated macromolecule, exhibiting diverse biological functions and chemical versatility[49,50]. Consequently, heparin-functionalized materials including surfaces, hydrogels[51], nanoparticles[52] have been engineered for applications such as protein/drug delivery, cancer nanomedicine, anti-coagulation and angiogenesis[23,24,53]. However, native heparin inherently suffers from chemical and structural heterogeneity, along with batch-to-batch variation, complicating control over its diverse biological activities[54].

Recent approaches to address these limitations include fractionating native heparin to isolate subsets with defined sulfation patterns[35,55], chemoenzymatic synthesis of structurally defined heparin oligosaccharides[56], recombinant expression of serglycin (a heparin proteoglycan) with post-translational modifications[57], and engineering heparin-mimetic derivatives using peptides[58], nanofibers[59], or sulfated polymer conjugates[60–62]. These strategies have predominantly focused on better controlling the extent and dynamics of anticoagulation[63], stabilizing growth factors[64], or stimulating cellular signaling for wound healing[65].

Here, we demonstrate a synthetic approach that replicates the angiogenic bioactivity of heparin without retaining its anticoagulant properties. Our engineered sulfated dextran hydrogels demonstrated a comparable ability to support vascularization as heparin-conjugated dextran gels, but crucially, without the bleeding risks typically associated with heparin. Using dextran, a homopolymer[66], as the base material offers additional advantages in generating functional biomaterials with controlled structure-property-performance, overcoming the molecular heterogeneity and batch variability inherent to natural heparin and other natural GAGs[29]. These findings highlight the importance of incorporating ECM-mimetic features into fully synthetic biomaterials to better recapitulate the complexity and functionality of biological systems.

Materials and Methods

Chemical synthesis of methacrylated dextran

Dextran (Mw~86 kDa, MP Biomedicals) was functionalized with methacrylate groups according to a previous published protocol[67]. Briefly, dextran (2.0 g) was dissolved in 10 mL anhydrous dimethyl sulfoxide (DMSO) with the addition of 0.2 g of base catalyst 4-dimethylamino pyridine (DMAP) and desired molar equivalent of glycidyl methacrylate (GMA, density = 1.042 g/mL at 25 °C). The solution mixture was kept constant at 45 °C and stirred for 24 hours before precipitating the final product *via* pipetting in drop-by-drop fashion of dark brown reaction solution to 100 mL ice-chilled

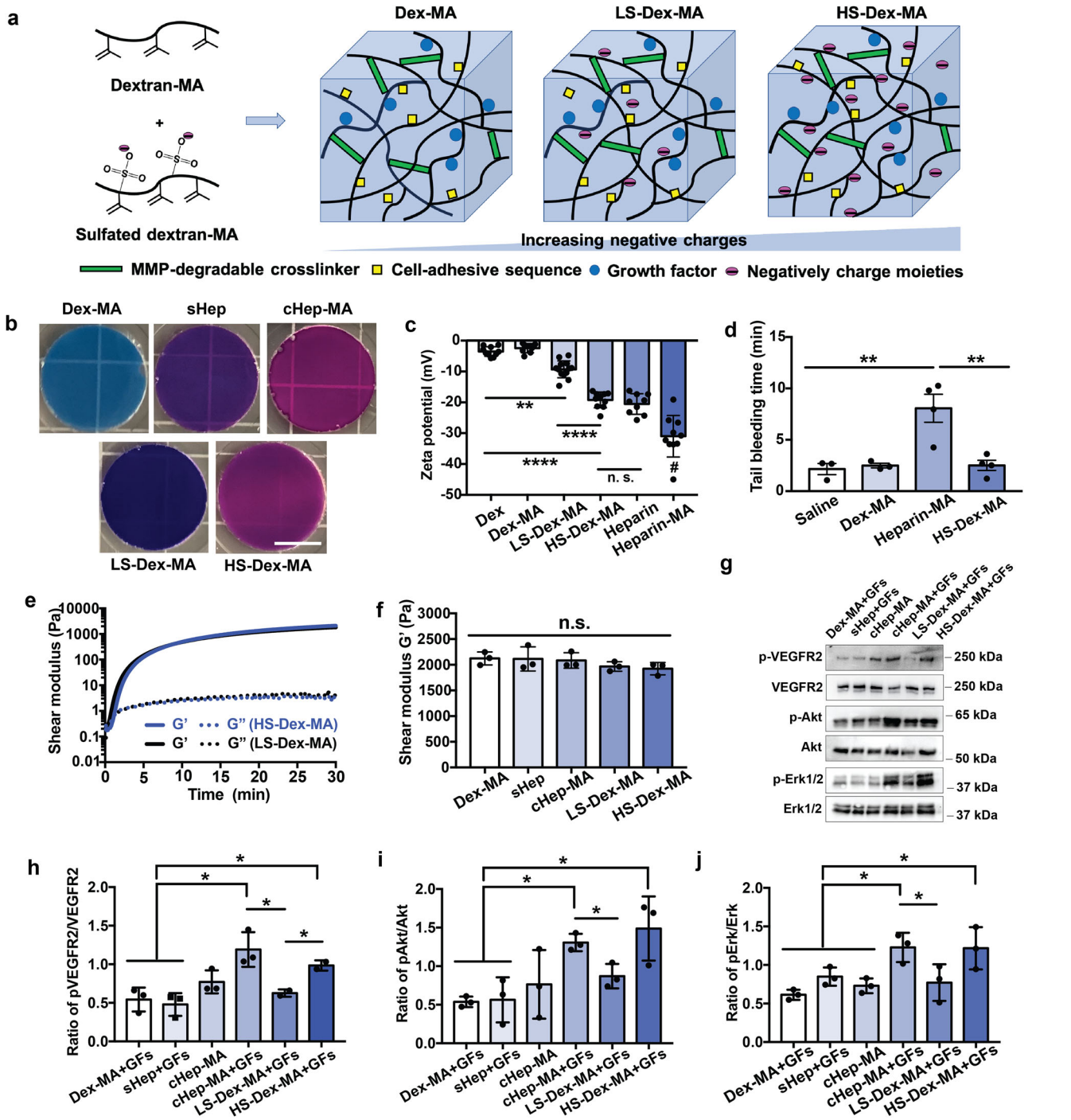

Fig. 2 | A synthetic heparin-mimetic hydrogel recapitulates pro-angiogenic property of native heparin without anti-coagulant activity. a Schematic of sulfated dextran hydrogel formation with increased negative charge density to mimic native heparin. Synthetic heparin-mimetic hydrogels were formulated by co-crosslinking Dex-MA and sulfated-Dex-MA (4 wt%, Dex-MA : sulfated-Dex-MA = 80 : 20, w/w(%)) in the presence of thiolated cell-adhesive peptide and di-thiol terminated MMP-cleavage peptide crosslinkers *via* a Michael-type addition reaction, identical crosslinking reaction employed in heparin-conjugated dextran gels. **b** Images of hydrogels with various compositions incubated in DMMB solution where the purple color is indicative of sulfate content, scale bar: 5 mm. **c** Zeta potential characterization of sulfated dextran with varying degrees of sulfation (LS-Dex-MA, $n = 13$ and HS-Dex-MA, $n = 10$) in comparison to unmodified dextran (Dex, $n = 10$), methacrylated dextran (Dex-MA, $n = 8$), native heparin ($n = 9$), and methacrylated heparin (Heparin-MA, $n = 10$). **d** Quantitative analysis of anticoagulant activity of saline control ($n = 3$), Dex-MA ($n = 3$), heparin-MA ($n = 4$), and sulfated-Dex-MA ($n = 4$) using a tail-bleeding assay. **e** Oscillatory shear rheology time course of sulfated dextran gels formulated with varying sulfation degrees, conducted at 37 °C with frequency of 6.28 rad/s and 1% strain, $n = 3$. **f** Hydrogel stiffness measurements using oscillatory shear rheology across various hydrogel compositions crosslinked at 4 wt% with an intermediate crosslinking ratio (1:0.75), showing no statistical differences among groups with a shear modulus (G' ~ 2000 Pa), $n = 3$. **g** Representative western blots of angiogenesis signaling pathways with HUVECs cultured on different hydrogel compositions. All material conditions were loaded with GFs during hydrogel formulation unless otherwise indicated. **h-j** Corresponding quantification of western blot associated with pVEGFR2, pAkt and pERK1/2 signaling in (**g**), $n = 3$. $^{**}P \le 0.01$, $^{****}P \le 0.0001$, # indicates that group is statistically significant compared to all other groups with $^{****}P \le 0.0001$, n. s. represents no statistical differences. Scatter dot plots with error bars represent means with standard deviations.

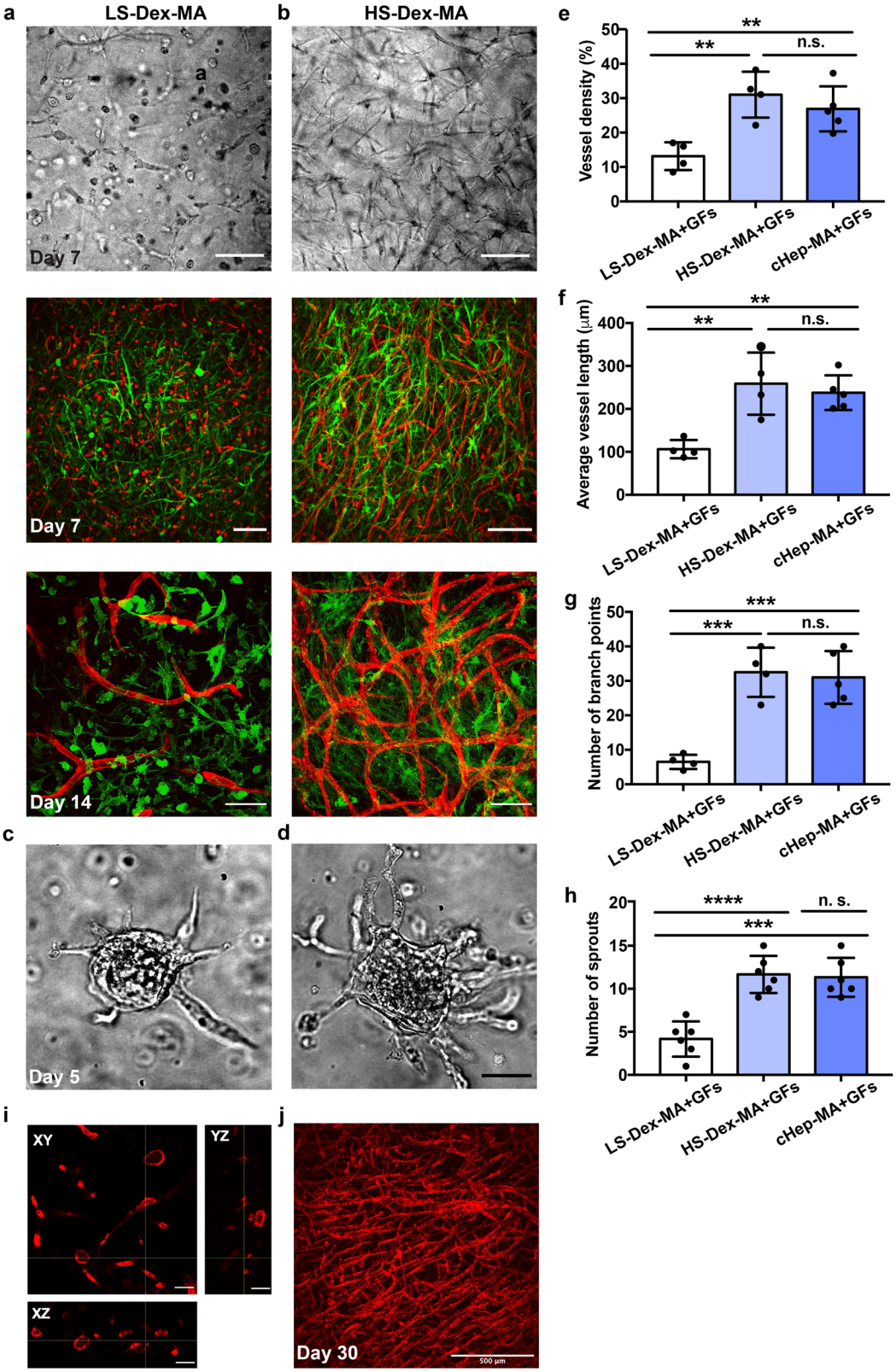

isopropanol. The crude product was then collected *via* centrifugation, re-dissolved in milli-Q water and dialyzed against milli-Q water (at 4 °C) for 3 days with 3 changes (4 L) daily before lyophilization. The degree of dextran methacrylate functionality was characterized *via* ^{1}H NMR spectroscopy, confirming a 70% modification (70 conjugated methacrylate groups per 100 dextran glucopyranose residues)[38].

Chemical synthesis of methacrylated heparin

Heparin (sodium salt from porcine intestinal mucosa, Mw~16 kDa, Sigma) was modified with methacrylate groups following a previously published method[68]. Briefly, 5% w/v heparin in milli-Q H_2O was prepared and reacted with 5-fold molar excess of methacrylic anhydride. The pH of the reaction mixture was adjusted to 8.5 using 5 N NaOH, and

Fig. 3 | Sulfated dextran as a synthetic heparin mimetic recapitulates pro-angiogenic property to support tissue vascularization in vitro. a, **b** Representative bright field and confocal fluorescent images of in vitro vascular network formation through co-culturing of Ruby-Lifeact-HUVECs and GFP-HDFs in sulfated dextran hydrogels (Dex-MA : sulfated-Dex-MA = 80 : 20, w/w(%)), (**a**) LS-Dex-MA: low sulfation dextran; (**b**) HS-Dex-MA: high sulfation dextran, $n = 4$, scale bar, 100 μm. **c**, **d** Representative bright field images of multicellular HUVEC-aggregates encapsulated in sulfated dextran hydrogels engineered with different sulfate degrees, scale bar: 200 μm. The degree of angiogenesis is quantified by comparing the number of endothelial sprouts per aggregate in different hydrogel compositions. HUVEC-aggregates were encapsulated at a density of ~1000 aggregates/mL and cultured in regular EGM-2 medium with medium changes every 2 days, and samples were fixed and imaged after 5 days, $n = 6$, $^{***}P < 0.001$. **e**–**h**) Quantitative assessment of in vitro vascular network structure at day 14, through quantifying (**e**) vessel density, $n = 4$, (**f**) average vessel length, $n = 4$, (**g**) number of branch points, $n = 4$; and (**h**) quantification of in vitro angiogenic sprouting *via* counting multicellular endothelial sprouts, $n = 6$. **i** Orthogonal views of vascular network formed in highly sulfated dextran hydrogel at day 14, with sections at different planes revealing the formation of lumen structures, scale bar, 50 μm. **j** Representative confocal fluorescent image of in vitro vascular network formation in highly sulfated dextran hydrogel at day 30, scale bar: 500 μm. $^{**}P < 0.01$, $^{***}P < 0.001$, $^{****}P < 0.0001$ and n.s. presents no statistical differences. Scatter dot plots with error bars represent means with standard deviations.

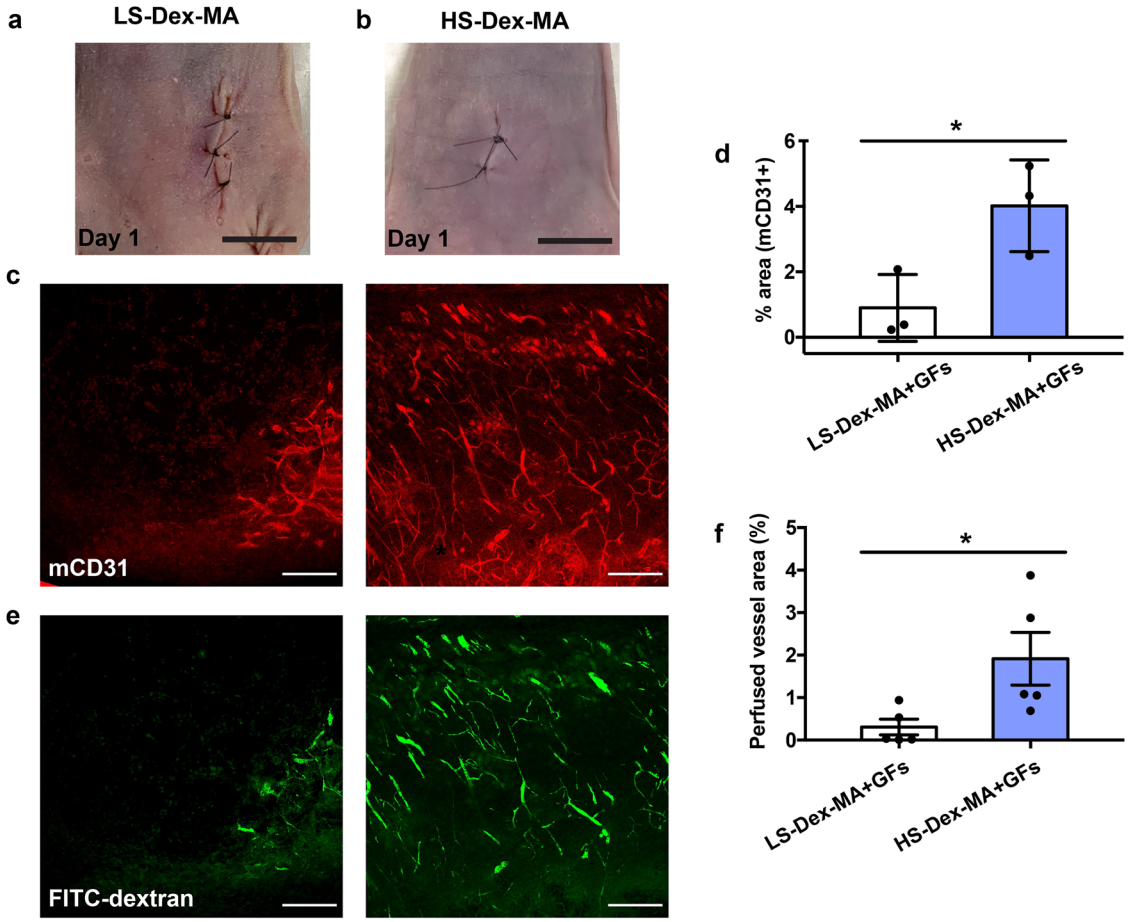

Fig. 4 | Sulfated dextran as a synthetic heparin mimetic circumvents the local bleeding side effects while retaining its pro-angiogenic property to support tissue vascularization in vivo. a, **b** Representative images showing implanted sulfated dextran hydrogels did not trigger local hemorrhage post implantation at day 1, scale bar, 1 cm. **c** Representative images of mouse CD31-stained tissue sections from sulfated dextran hydrogel harvested on day 14, scale bar, 200 μm. **d** Quantitative analysis of host blood vessels invading into sulfated dextran gels measured as the percentage of mCD31 positive area, $n = 3$. **e** Representative images of FITC-dextran signals in sections of sulfated dextran hydrogels with FITC-dextran (70 kDa) intravenously injected prior to harvesting in vivo tissue samples at day 14, scale bar, 200 μm. **f** Percentage of perfused host vessels quantified by FITC-dextran (70 kDa) positive area, $n = 5$, $^{*}P < 0.05$. Scatter dot plots with error bars represent means with standard deviations.

the reaction was proceeded overnight at 4 °C. The product was then precipitated in 95% ethanol, dried and dialyzed (3000 Mw cutoff) for 3 days in milli-Q H_2O and lyophilized. The degree of methacrylation was characterized *via* ^{1}H NMR spectroscopy, confirming an average of 16% methacrylation.

Chemical synthesis of sulfated dextran

Methacrylate-modified dextran was modified following a previously published method[44]. Briefly, Dex-MA (0.5 wt%) was dissolved in *N, N*-dimethylformadmide (DMF) with various amount of SO_3/DMF complex added to the reaction solution to achieve a range of molar ratio of SO_3/DMF : Dex-MA repeat unit (e.g., 1:1, 5:1, and 10:1, mol/mol), a means to tune the degree of sulfation in final product. The solution mixture was reacted under N_2 at room temperature for 1 h followed by dialysis (10000 Da Mw cutoff) against milli-Q H_2O at 4 °C for 7 days and lyophilized.

Dextran-based hydrogel formulation

3D dextran-based hydrogels were prepared via mixing Dex-MA (100 mg/mL) with 8 mM thiolated RGD peptide (cell-adhesive sequence: CGRGDS; non-adhesive control: CGRGES, Aapptec) in the presence of matrix

metalloproteinase (MMP)-cleavable dithiol-containing crosslinker peptide (degradable crosslinker: CGPQGIAGQGCR, derived from collagen I; slow-degradable control: CGPQGPAGQGCR, Aapptec) in M199 media containing sodium bicarbonate (3.5% w/v) and HEPES (10 mM). To formulate heparinized dextran hydrogels, Dex-MA precursor solution was mixed with either heparin-MA (100 mg/mL) or non-modified heparin (100 mg/mL) at 90:10 w/w ratio. To formulate sulfated dextran hydrogels, Dex-MA precursor solution was mixed with sulfated Dex-MA (100 mg/mL, at low and high sulfation degree) at 80:20 w/w ratio. The pH of the solution was then adjusted approximately to 8 with NaOH (1 M) to initiate hydrogel formation through Michael-type addition reaction and maintained for 45 minutes at 37 °C for complete gelation. To formulate hydrogels with different stiffness, bulk material solution concentration or MMP-labile peptide crosslinker density can be tuned independent of other material parameters during crosslinking. Hydrogels were formulated using multiple independently synthesized batches of Dex-MA, Hep-MA, and sulfated Dex-MA to ensure reproducibility and account for potential batch-to-batch variability, with each condition tested in at least 4 independent biological experiments.

Mechanical characterization *via* oscillatory rheology

Bulk hydrogel mechanical properties were measured using a strain-controlled Discovery HR-2 oscillatory shear rheometer (TA Instruments, New Castle, DE), with a 20 mm diameter cone-on plate geometry, 2° cone angle, and at a 62 μm gap distance at 37 °C. Hydrogels with various compositions were prepared as described above. Hydrogel precursor solutions were deposited onto the rheometer Peltier plate for in situ mechanical stiffness measurements. To determine hydrogel formation and gelation kinetics, a time sweep was first performed at a constant 6 rad/s frequency, 1% strain; followed by a frequency sweep conducted over a logarithmic scale from 0.1 to 100 rad/s at a fixed strain amplitude of 1% to confirm the mechanical stability of resulting hydrogels. Data were collected from multiple measurements of four independent samples.

Hydrogel swelling

Dextran hydrogels (~ 200 μL, 4 wt% polymer concentration) with various compositions were prepared as described above and their in situ weights after crosslinking were measured. Samples were then immersed in PBS and hydrogel swollen weights were measured after 24 h incubation at 37 °C. The swelling degree of hydrogels is calculated by dividing swollen weight over in situ weight.

In situ hydrogel degradation

Dextran-based hydrogels formulated with degradable crosslinker (CGPQGIAGQGCR, derived from collagen I, 200 μL starting volume per gel) were incubated in PBS for 24 h at 37 °C to assess the initial equilibrium swollen weight. The swollen hydrogels were then transferred to a 0.2 mg/mL collagenase solution in PBS and the hydrogel weight was continuously monitored over 72 h. Control hydrogels include degradable gels incubated in PBS without collagenase and gels formulated with low degradable crosslinker sequence (CGPQGPAGQGCR) in the presence of 0.2 mg/mL collagenase.

Zeta potential measurements

Various polysaccharide-based solutions were prepared at a concentration of 100 mg/mL in MilliQ H_2O and approximate 800 μL solution was loaded into a disposable cuvette. The analyses were conducted at room temperature using NanoBrook ZetaPlus apparatus (Brookhaven Instruments, Holtsville, NY). The zeta potential of polysaccharide solutions was measured using the electrophoretic light scattering spectrophotometer of the instrument.

Dimethylmethylene blue assay

To confirm the successful incorporation and visualization of sulfate residues in hydrogels, 200 μL hydrogels with various compositions were prepared (as described above), immersed in PBS at 37 °C for 24 h to reach equilibrium swelling, and then incubated in a DMMB solution (16 mg dimethylmethylene blue, 3.04 g glycine, 2.37 g NaCl and 95 mL 0.1 M HCl in 1 L MilliQ H_2O, with a final solution pH approximate ~3.0) overnight at 37 °C. Hydrogels were then washed with PBS and photographed.

Cell culture and 3D encapsulation

Human dermal fibroblasts labeled with GFP (HDFs, passage 7-9) were cultured in fully supplemented fibroblast growth medium-2 (FGM-2) (Lonza). HUVECs labeled with Ruby-LifeAct (HUVECs, passage 2-7) were cultured in fully supplemented endothelial cell growth medium-2 (EGM-2) (Lonza). For cell culture in 3D hydrogels, endothelial multicellular aggregates were fabricated using microwell culture plates (AggreWell^{TM}400, Stemcell Technologies, Vancouver, Canada) according to standard protocols and were encapsulated at ~500 aggregates for each hydrogel composition for angiogenesis assay. For the vasculogenesis assay, GFP-HDFs and Ruby-LifeAct-HUVECs were encapsulated in the pH adjusted hydrogel precursor solutions at a final concentration of ~9 million cells/mL (GFP-HDF:Ruby-LifeAct-HUVECs = 1:2, cell density). 50 μL of the cell-containing hydrogel solution was then deposited onto uncoated glass-bottomed 35 mm dishes (MaTek Corporation, P35G-1.0–20) and allowed to polymerize for 45 min in 37 °C incubator before adding cell culture medium (EMG-2). HUVEC-aggregate/HUVEC-HDF co-culture hydrogels were maintained at 37 °C and 5% CO_2 in a humidified incubator with cell medium changes every two days. Cell lines were tested for mycoplasma contamination using MycoAlert Mycoplasma Detection Kit (Lonza).

Western blot

HUVECs were seeded on 2D hydrogels substrates (formulated with identical material compositions for 3D cell encapsulations) for 20–24 h. Cells were then washed twice with ice cold PBS and lysed in RIPA buffer (1% TritonX-100, 0.1% SDS, 1% Sodium deoxycholate, 50 mM Tris-HCl, pH 7.4, 150 mM NaCl, 2 mM EDTA, and 1x protease halt (Thermo Fischer Scientific, Waltham, MA). Cell lysate aliquots with equal amounts of total protein (as measured using the Pierce Coomassie protein assay reagent) were separated on an SDS-PAGE gel, transferred to PVDF, blocked in 5% milk or 5% BSA (phospho-proteins) and subjected to Western blot analysis using antibodies from Cell Signaling (pVEGFR2, 2478; VEGFR2, 2479; pERK1/2, #4370; ERK1/2, #4695; pAkt, #9271; Akt, #9272; and GAPDH, #5174). The blots were developed using ECL Western blot detection reagents (Pierce), and the signal was detected on iBright^{TM} CL1500 Imaging System (ThermoFisher Scientific, Waltham, MA).

Tail bleeding assay

The tail-bleeding assay was performed to determine the anti-coagulation property of heparin, Dex-MA and sulfated-Dex-MA. Briefly, an osmotic minipump (ALZET, model 1007D, Cupertino, CA) loaded with 100 μL of Hep-MA, Dex-MA and sulfated-Dex-MA (stock solution concentration at 100 mg/ml) was implanted under the dorsal skin 36 hours before the assay was performed. On the day of the assay, the animals were anaesthetized using an isoflurane nebulizer, which was maintained throughout the procedure. A distal 7-mm segment of the tail was amputated with a scalpel. Immediately after, the animal was placed in prone position with the tail vertically immersed in isotonic saline pre-warmed to 37 °C and the bleeding time was recorded using a timer for a maximum of 20 min. The animal was then euthanized by overdose of isoflurane and cervical dislocation. All animal procedures were performed at the Charles River campus animal facility, Boston University, under a protocol approved by the Institutional Animal Care and Use Committee. All experiments pertaining to this investigation conformed to the "Guide for the Care and Use of Laboratory Animals". We have complied with all relevant ethical regulations for animal use.

In vivo angiogenesis assay and quantifications

To evaluate in vivo cell invasion and angiogenesis, hydrogels formulated with various compositions (e.g., Dex-MA+GFs, sHep+GFs, cHep-MA +GFs, cHep-MA, LS-Dex-MA+GFs, and HS-Dex-MA+GFs) were

introduced to the abdominal subcutaneous space of mouse models either through injections or implantations. Recombinant mouse growth factors, $VEGF_{164}$ and bFGF (R&D System), were incorporated during hydrogel formation at the concentrations of 18.5 nM and 5.2 nM, respectively. Mice (six-to-eight-week-old female C57BL/6NTac or BALB/c nude mice, CrTac:NCr-Foxn1nu strain, JAX or Taconic) were used in this study. The animals were anaesthetized using an isoflurane nebulizer, which was maintained throughout the procedure. For injections, the hydrogel solution (100 µL) was directly injected subcutaneously before they polymerized. For implantation, the hydrogel was pre-formed in 6 mm-diameter, 4 mm-height PDMS molds (~ 60 µL in volume) before being extracted out of the mold and inserted into the subcutaneous pocket. Standard septic surgery procedures were followed by appropriate deep anesthesia using standard isoflurane throughout the procedures following by appropriate analgesic administrations. Two weeks after the injection or implantation, lysine-fixable fluorescein-conjugated dextran (FITC-dextran, 100 µL, Mw~70 kDa, 10 mg mL^{-1} in saline; Invitrogen) was injected retro-orbitally, five minutes post-injection, animals were euthanized by cervical dislocation under anesthesia, and hydrogel samples were harvested. All hydrogel samples were fixed in 4% paraformaldehyde (PFA) in PBS at 4 °C overnight, washed in PBS at 4 °C overnight and immersed in 30% sucrose in PBS at 4 °C for at least 2 days. Hydrogel samples were then embedded in optimum cutting temperature compound (OCT, Tissue-Tek® or Fisherbrand) in the orientation that the skin side is vertical so that the tissue cross-sections would include the skin to mark the hydrogel margin. From the middle region of each hydrogel sample, 50 µm-thick sections were collected on Superfrost Plus slides (Fisherbrand) for immunostaining and analysis. The use of different mouse species for male and female groups was based on animal availability at the time of conducting the experiments. A total of number of 120 mice used in this study. No significant differences were observed in the degree of host vessel invasion or angiogenesis in vivo, which is primarily dependent on hydrogel compositions rather than mouse species or sex.

To demonstrate blood vessels, tissue sections were stained with mouse CD31 (1:100, 4 °C overnight, clone MEC13.3, BD Pharmingen, #561814) followed by AlexaFluor 647 anti-rat antibody (1:500, RT 1 h) and DAPI staining. To quantify invaded blood vessels and their perfusion, fluorescent images of mCD31 and FITC-dextran signals for the full 50 μm tissue section of each hydrogel sample were acquired with a Leica Microscope Objective (HCX Apo 10X/0.3 W) on an upright Leica TCS SP8 multiphoton microscope with the same setting in a randomized but not overlapping fashion. The percentage (%) total area of mCD31 or FITC-dextran signal was then determined using ImageJ and the average of the fluorescent images for each hydrogel sample represents that hydrogel sample.

Fluorescent staining and microscopy

HDFs and HUVECs co-cultured in various Dex-MA hydrogels were fixed with 4% paraformaldehyde (PFA) at room temperature for 30 minutes. To visualize the organization of the actin cytoskeleton, cells were stained with phalloidin-Alexa Fluor 488, 1:1000 (Life Technologies, Carlsbad, CA) for overnight with nuclei counterstained with Hoechst (1:1000) for 1 hour at room temperature on next day. For immunostaining, fixed samples were first permeabilized with 0.1% Triton X-100 for 30 min and then blocked with 5 wt% goat serum in 0.01% Triton X-100 for 3 h, followed by incubating with primary antibody (laminin: 1:500 rabbit polyclonal to laminin (Abcam, ab23753); CD31: 1:500 mouse monoclonal anti-CD31 I (Abcam, ab9498)) overnight and secondary antibody (1:1000 Alexa Fluor 567 goat anti-rabbit IgG (H + L) (Life Technologies) and 1:1000 Alexa Fluor 488 goat anti-mouse IgG (H + L) and) simultaneously for 1 h at 4 °C. Fluorescent images were acquired using a Leica SP8 laser scanning confocal microscope (Leica Microsystems) with a Leica HC FLUOTAR L 25x/0.95 W VISIR or a Leica HCX APO L 10x/0.30 W U-VI objective. Composite images were acquired in spatial sequence using equal laser intensity and detector gain. Unless otherwise specified, images are manually processed and presented as maximum intensity projections using ImageJ.

Statistics and reproducibility

Statistical analysis was performed in GraphPad Prism 7, where data were first tested for normality using the Shapiro-Wilk test before performing one-way ANOVA, followed by Tukey-HSD post-hoc test on all datasets. Dual group analysis was performed using an unpaired Student's t-test. For experiments involving angiogenic sprouting assay, multicellularity vascular network formation experiments, and in vivo tissue vascularization characterization, results are presented in scatter blot plots containing mean ± standard deviation, $n \geq 4$ samples were analyzed. Statistical significance is indicated by *, **, *** or **** which corresponds to P values ≤ 0.05, 0.01, 0.001 or 0.0001, and n. s. stands for statistically insignificant.

Reporting summary

Further information on research design is available in the Nature Portfolio Reporting Summary linked to this article.

Data availability

All data generated or analyzed to support the findings of current study are included in this published article and its supplementary information files. Numerical source data underlying all figures in the manuscript can be found in supplementary data file.

Received: 3 May 2025; Accepted: 24 September 2025;
Published online: 14 November 2025

References

1. Khademhosseini, A. & Langer, R. A decade of progress in tissue engineering. *Nat. Protoc.* **11**, 1775–1781 (2016).
2. Song, H.-H. G., Rumma, R. T., Ozaki, C. K., Edelman, E. R. & Chen, C. S. Vascular tissue engineering: progress, challenges, and clinical promise. *Cell Stem Cell* **22**, 340–354 (2018).
3. Zhao, N., Pessell, A. F., Zhu, N. & Searson, P. C. Tissue-engineered microvessels: a review of current engineering strategies and applications. *Adv. Healthc. Mater.* **13**, 2303419 (2024).
4. Lee, G. et al. PCL-fibrin-alginate hydrogel based cell co-culture system for improving angiogenesis and immune modulation in limb ischemia. *Colloids Surf. B Biointerfaces* **250**, 114553 (2025).
5. Khatoon, F., Narula, A. K. & Sehgal, P. Efficacy of collagen based biomaterials in diabetic foot ulcer wound healing. *Eur. Polym. J.* **217**, 113345 (2024).
6. Simińska-Stanny, J., Podstawczyk, D., Delporte, C., Nie, L. & Shavandi, A. Hyaluronic acid role in biomaterials prevascularization. *Adv. Healthc. Mater.* **13**, 2402045 (2024).
7. Friend, N. E. et al. Biofabrication and characterization of vascularizing peg-norbornene microgels. *J. Biomed. Mater. Res. Part A* **113**, e37900 (2025).
8. Zhang, Y. et al. A versatile chitosan-based hydrogel accelerates infected wound healing via bacterial elimination, antioxidation, immunoregulation, and angiogenesis. *Adv. Healthc. Mater.* **13**, 2400318 (2024).
9. Briquez, P. S. et al. Design principles for therapeutic angiogenic materials. *Nat. Rev. Mater.* **1**, 15006 (2016).
10. Li, H. et al. Progress in biomaterials-enhanced vascularization by modulating physical properties. *ACS Biomater. Sci. Eng.* **11**, 33–54 (2025).
11. Margolis, E. A., Friend, N. E., Rolle, M. W., Alsberg, E. & Putnam, A. J. Manufacturing the multiscale vascular hierarchy: progress toward solving the grand challenge of tissue engineering. *Trends Biotechnol.* **41**, 1400–1416 (2023).
12. Shan, B.-H. & Wu, F.-G. Hydrogel-based growth factor delivery platforms: strategies and recent advances. *Adv. Mater.* **36**, 2210707 (2024).
13. Libby, J. R., Royce, H., Walker, S. R. & Li, L. The role of extracellular matrix in angiogenesis: Beyond adhesion and structure. *Biomater. Biosyst.* **15**, 100097 (2024).

14. van Velthoven, M. J. J. et al. Growth factor immobilization to synthetic hydrogels: bioactive bFGF-functionalized polyisocyanide hydrogels. *Adv. Healthc. Mater.* **12**, 2301109 (2023).
15. Rana, D. et al. Spatial control of self-organizing vascular networks with programmable aptamer-tethered growth factor photopatterning. *Mater. Today Bio* **19**, 100551 (2023).
16. Leslie-Barbick, J. E., Moon, J. J. & West, J. L. Covalently-immobilized vascular endothelial growth factor promotes endothelial cell tubulogenesis in poly(ethylene glycol) diacrylate hydrogels. *J. Biomater. Sci. Polym. Ed.* **20**, 1763–1779 (2009).
17. Chiu, L. L. Y. & Radisic, M. Scaffolds with covalently immobilized VEGF and Angiopoietin-1 for vascularization of engineered tissues. *Biomaterials* **31**, 226–241 (2010).
18. Masters, K. S. Covalent growth factor immobilization strategies for tissue repair and regeneration. *Macromol. Biosci.* **11**, 1149–1163 (2011).
19. Jensen, B. E. B., Edlund, K. & Zelikin, A. N. Micro-structured, spontaneously eroding hydrogels accelerate endothelialization through presentation of conjugated growth factors. *Biomaterials* **49**, 113–124 (2015).
20. Weaver, J. D. et al. Vasculogenic hydrogel enhances islet survival, engraftment, and function in leading extrahepatic sites. *Sci. Adv.* **3**, e1700184 (2017).
21. Isik, M. et al. 3D printing of extracellular matrix-based multicomponent, all-natural, highly elastic, and functional materials toward vascular tissue engineering. *Adv. Healthc. Mater.* **12**, 2203044 (2023).
22. Jiang, S., Wise, S. G., Kovacic, J. C., Rnjak-Kovacina, J. & Lord, M. S. Biomaterials containing extracellular matrix molecules as biomimetic next-generation vascular grafts. *Trends Biotechnol.* **42**, 369–381 (2024).
23. Sakiyama-Elbert, S. E. Incorporation of heparin into biomaterials. *Acta Biomater.* **10**, 1581–1587 (2014).
24. Liang, Y. & Kiick, K. L. Heparin-functionalized polymeric biomaterials in tissue engineering and drug delivery applications. *Acta Biomater.* **10**, 1588–1600 (2014).
25. Nazarzadeh Zare, E. et al. Biomedical applications of engineered heparin-based materials. *Bioact. Mater.* **31**, 87–118 (2024).
26. Folkman, J. Regulation of angiogenesis: a new function of heparin. *Biochem. Pharmacol.* **34**, 905–909 (1985).
27. Peysselon, F. & Ricard-Blum, S. Heparin–protein interactions: from affinity and kinetics to biological roles. Application to an interaction network regulating angiogenesis. *Matrix Biol.* **35**, 73–81 (2014).
28. Capila, I. & Linhardt, R. J. Heparin–protein interactions. *Angew. Chem. Int. Ed.* **41**, 390–412 (2002).
29. Rnjak-Kovacina, J., Tang, F., Whitelock, J. M. & Lord, M. S. Glycosaminoglycan and proteoglycan-based biomaterials: current trends and future perspectives. *Adv. Healthc. Mater.* **7**, 1701042 (2018).
30. Elia, R. et al. Stimulation of in vivo angiogenesis by in situ crosslinked, dual growth factor-loaded, glycosaminoglycan hydrogels. *Biomaterials* **31**, 4630–4638 (2010).
31. Tsurkan, M. V. et al. Defined Polymer–Peptide Conjugates to Form Cell-Instructive starPEG–Heparin Matrices In Situ. *Adv. Mater.* **25**, 2606–2610 (2013).
32. Song, Y. et al. Absolute pharmacokinetics of heparin in primates. *Carbohydr. Polym.* **311**, 120779 (2023).
33. Oliveira, S. N. M. C. G. et al. Global use of bovine heparin: challenges and opportunities. *Proteoglycan Res.* **3**, e70025 (2025).
34. Chiasakul, T., Mullier, F., Lecompte, T., Nguyen, P. & Cuker, A. Laboratory monitoring of heparin anticoagulation in hemodialysis: rationale and strategies. *Semin. Nephrol.* **43**, 151477 (2023).
35. Limasale, Y. D. P., Atallah, P., Werner, C., Freudenberg, U. & Zimmermann, R. Tuning the local availability of VEGF within glycosaminoglycan-based hydrogels to modulate vascular endothelial cell morphogenesis. *Adv. Funct. Mater.* **30**, 2000068 (2020).
36. Martwiset, S., Koh, A. E. & Chen, W. Nonfouling characteristics of dextran-containing surfaces. *Langmuir* **22**, 8192–8196 (2006).
37. Sun, G. & Mao, J. J. Engineering dextran-based scaffolds for drug delivery and tissue repair. *Nanomedicine* **7**, 1771–1784 (2012).
38. Li, L. et al. A protein-adsorbent hydrogel with tunable stiffness for tissue culture demonstrates matrix-dependent stiffness responses. *Adv. Funct. Mater.* **34**, 2309567 (2024).
39. Lutolf, M. P. et al. Synthetic matrix metalloproteinase-sensitive hydrogels for the conduction of tissue regeneration: engineering cell-invasion characteristics. *Proc. Natl. Acad. Sci. USA* **100**, 5413–5418 (2003).
40. Song, H.-H. G. et al. Transient support from fibroblasts is sufficient to drive functional vascularization in engineered tissues. *Adv. Funct. Mater.* **30**, 2003777 (2020).
41. Barrasa-Ramos, S., Dessalles, C. A., Hautefeuille, M. & Barakat, A. I. Mechanical regulation of the early stages of angiogenesis. *J. R. Soc. Interface* **19**, 20220360 (2022).
42. Folkman, J., Taylor, S. & Spillberg, C. The role of heparin in angiogenesis. *Ciba Found. Symp.* **100**, 132–149 (1983).
43. da Costa, D., Reis, R. L. & Pashkuleva, I. Sulfation of Glycosaminoglycans and Its Implications in Human Health and Disorders. *Annu. Rev. Biomed. Eng.* **19**, 1–26 (2017).
44. Purcell, B. P. et al. Incorporation of sulfated hyaluronic acid macromers into degradable hydrogel scaffolds for sustained molecule delivery. *Biomater. Sci.* **2**, 693–702 (2014).
45. Gospodarowicz, D. & Cheng, J. Heparin protects basic and acidic FGF from inactivation. *J. Cell. Physiol.* **128**, 475–484 (1986).
46. Mouw, J. K., Ou, G. & Weaver, V. M. Extracellular matrix assembly: a multiscale deconstruction. *Nat. Rev. Mol. Cell Biol.* **15**, 771–785 (2014).
47. Humphrey, J. D., Dufresne, E. R. & Schwartz, M. A. Mechanotransduction and extracellular matrix homeostasis. *Nat. Rev. Mol. Cell Biol.* **15**, 802–812 (2014).
48. Marchand, M., Monnot, C., Muller, L. & Germain, S. Extracellular matrix scaffolding in angiogenesis and capillary homeostasis. *Semin. Cell Dev. Biol.* **89**, 147–156 (2019).
49. Casu, B. & Lindahl, U. B. T.-A. in C. C. and B. Structure and biological interactions of heparin and heparan sulfate. in vol. 57, 159–206 (Academic Press, 2001).
50. Linhardt, R. J. & Claude, S. Hudson Award Address in Carbohydrate Chemistry. Heparin: Structure and Activity. *J. Med. Chem.* **46**, 2551–2564 (2003).
51. Lu, D. et al. VEGF loading heparinized hyaluronic acid macroporous hydrogels for enhanced 3D endothelial cell migration and vascularization. *Biomater. Adv.* **167**, 214094 (2025).
52. Cheng, K. et al. Heparin-loaded hierarchical fiber/microsphere scaffolds for anti-inflammatory and promoting wound healing. *Smart Mater. Med.* **5**, 240–250 (2024).
53. He, C. et al. Heparin-based and heparin-inspired hydrogels: size-effect, gelation and biomedical applications. *J. Mater. Chem. B* **7**, 1186–1208 (2019).
54. Freedman, M. D. Pharmacodynamics, clinical indications, and adverse effects of heparin. *J. Clin. Pharmacol.* **32**, 584–596 (1992).
55. Gama, C. I. et al. Sulfation patterns of glycosaminoglycans encode molecular recognition and activity. *Nat. Chem. Biol.* **2**, 467–473 (2006).
56. Xu, Y. et al. Chemoenzymatic synthesis of homogeneous ultralow molecular weight heparins. *Science* **334**, 498–501 (2011).
57. Farrugia, B. L., Lord, M. S., Melrose, J. & Whitelock, J. M. Can we produce heparin/heparan sulfate biomimetics using “mother-nature” as the gold standard? *Molecules* **20**, 4254–4276 (2015).

58. Fan, F. et al. Peptide-based organic-inorganic hybrid self-assemblies for ultrasensitive and visual detection of heparin. *Adv. Funct. Mater.* **34**, 2314832 (2024).
59. Fahad, M. A. A. l. et al. Small-diameter vascular graft composing of core-shell structured micro-nanofibers loaded with heparin and VEGF for endothelialization and prevention of neointimal hyperplasia. *Biomaterials* **306**, 122507 (2024).
60. Kim, S. H. & Kiick, K. L. Heparin-mimetic sulfated peptides with modulated affinities for heparin-binding peptides and growth factors. *Peptides* **28**, 2125–2136 (2007).
61. Paluck, S. J., Nguyen, T. H. & Maynard, H. D. Heparin-mimicking polymers: synthesis and biological applications. *Biomacromolecules* **17**, 3417–3440 (2016).
62. Lee, S. S. et al. Sulfated glycopeptide nanostructures for multipotent protein activation. *Nat. Nanotechnol.* **12**, 821–829 (2017).
63. Nahain, A. A. et al. Anticoagulant heparin mimetics via RAFT polymerization. *Biomacromolecules* **21**, 1009–1021 (2020).
64. Nguyen, T. H. et al. A heparin-mimicking polymer conjugate stabilizes basic fibroblast growth factor. *Nat. Chem.* **5**, 221–227 (2013).
65. Yergoz, F. et al. Heparin mimetic peptide nanofiber gel promotes regeneration of full thickness burn injury. *Biomaterials* **134**, 117–127 (2017).
66. Bubli, S. Y. et al. Inducing an LCST in hydrophilic polysaccharides via engineered macromolecular hydrophobicity. *Sci. Rep.* **13**, 14896 (2023).
67. van Dijk-Wolthuis, W. N. E. et al. Synthesis, characterization, and polymerization of glycidyl methacrylate derivatized dextran. *Macromolecules* **28**, 6317–6322 (1995).
68. Benoit, D. S. W., Durney, A. R. & Anseth, K. S. The effect of heparin-functionalized PEG hydrogels on three-dimensional human mesenchymal stem cell osteogenic differentiation. *Biomaterials* **28**, 66–77 (2007).

Acknowledgements

The authors acknowledge the support from the Department of Biomedical Engineering Core Facilities and the Biological Design Center at Boston University. The authors also acknowledge the financial support from the National Institute of Health EB000262 (CSC), EB008396 (CSC), and the National Science Foundation Science and Technology Center for Engineering Mechanobiology grant CMMI-1548571 (CSC). L.L. acknowledges the financial support from the New Hampshire BioMade provided by the National Science Foundation through EPSCoR Research Infrastructure Improvement Award IIA 1757371 (LL), the National Institute of General Medical Sciences of the National Institute of Health, P20GM113131 (LL) and R35GM155450 (LL).

Author contributions

L.L. and J.Y. contributed equally to this project. L.L. and C.S.C. designed the materials. L.L., J.Y., J.E., S.N.B. and C.S.C. conceived the study and designed the experiments. L.L., J.Y., L.P. and J.L.B. performed all experiments and data analysis. L.L., J.Y., J.L.B., J.E. and C.S.C. wrote the manuscript with input from all authors. C.S.C. supervised the project.

Competing interests

C.S.C. is a founder and own shares of Satellite Biosciences and RopirioTherapeutics. S.N.B. holds equity in Amplifyer Bio, Catalio Capital, Earli, Impilo Therapeutics, Matrisome Bio, Ochre Bio, Port Therapeutics, RopirioTherapeutics, Satellite Bio, Sunbird Bio, and Vertex Pharmaceuticals, advises Danaher, Moderna, Pictet, and Xilio Therapeutics, and receives sponsored research funding from Johnson & Johnson, and Owlstone Medical. The remaining authors declare no competing interests. The authors declare that they have no known competing financial interests or personal relationships that could have appeared to influence the work reported in this paper.

Additional information

Supplementary information The online version contains supplementary material available at https://doi.org/10.1038/s42003-025-08946-4.

Correspondence and requests for materials should be addressed to Linqing Li or Christopher S. Chen.

Peer review information *Communications Biology* thanks Renato Navarro, Ande Marini, and the other, anonymous, reviewer for their contribution to the peer review of this work. Primary Handling Editors: Ngan Huang and Joao Valente. A peer review file is available.